ARTICLE IN PRESS

Nature Communications

https://doi.org/10.1038/s41467-026-71918-7

Article in Press

Developmental disinhibition gates language lateralization in childhood

Received: 16 July 2025

Accepted: 31 March 2026

Cite this article as: Ismail, M.M., Momi, D., Wang, Z. *et al.* Developmental disinhibition gates language lateralization in childhood. *Nat Commun* (2026). https://doi.org/10.1038/s41467-026-71918-7

Minarose M. Ismail, Davide Momi, Zheng Wang, Sorenza P. Bastiaens, M. Parsa Oveisi, Hansel M. Greiner, Donald J. Mabbott, John D. Griffiths & Darren S. Kadis

We are providing an unedited version of this manuscript to give early access to its findings. Before final publication, the manuscript will undergo further editing. Please note there may be errors present which affect the content, and all legal disclaimers apply.

If this paper is publishing under a Transparent Peer Review model then Peer Review reports will publish with the final article.

ARTICLE IN PRESS

© The Author(s) 2026. **Open Access** This article is licensed under a Creative Commons Attribution-NonCommercial-NoDerivatives 4.0 International License, which permits any non-commercial use, sharing, distribution and reproduction in any medium or format, as long as you give appropriate credit to the original author(s) and the source, provide a link to the Creative Commons licence, and indicate if you modified the licensed material. You do not have permission under this licence to share adapted material derived from this article or parts of it. The images or other third party material in this article are included in the article's Creative Commons licence, unless indicated otherwise in a credit line to the material. If material is not included in the article's Creative Commons licence and your intended use is not permitted by statutory regulation or exceeds the permitted use, you will need to obtain permission directly from the copyright holder. To view a copy of this licence, visit http://creativecommons.org/licenses/by-nc-nd/4.0/.

Developmental Disinhibition Gates Language Lateralization in Childhood

Minarose M. Ismail[1,2], Davide Momi[3], Zheng Wang[3], Sorenza P. Bastiaens[3,4], M. Parsa Oveisi[3,4], Hansel M. Greiner[5], Donald J. Mabbott[2,6], John D. Griffiths[3,4,7*], Darren S. Kadis[1,2*]

[1]Department of Physiology, University of Toronto, Toronto, Canada
[2]Neurosciences & Mental Health, The Hospital for Sick Children, Toronto, Canada
[3]Krembil Centre for Neuroinformatics, Centre for Addiction and Mental Health, Toronto, Canada
[4]Institute of Medical Sciences, University of Toronto, Toronto, Canada
[5]Department of Pediatrics, College of Medicine, University of Cincinnati, Cincinnati, USA
[6]Department of Psychology, University of Toronto, Toronto, Canada
[7]Department of Psychiatry, University of Toronto, Toronto, Canada

*Co-corresponding authors

***Please address correspondence to: Dr. Darren S. Kadis** Neurosciences and Mental Health, Hospital for Sick Children 686 Bay Street, Toronto, ON M5G 0A4, Canada Email: darren.kadis@sickkids.ca Phone: +1 (416) 813-7654 ext. 308283 **or: Dr. John D. Griffiths** Krembil Centre for Neuroinformatics, Centre for Addiction & Mental Health 250 College Street, Toronto, ON M5T 1L8, Canada Email: john.griffiths@camh.ca Phone: +1 (416) 535-8501 ext: 30251

ARTICLE IN PRESS

Abstract

Hemispheric specialization is a hallmark of brain organization, yet how functionally specialized circuits develop remains unclear. In humans, the developmental shift toward left-hemisphere dominance for language offers a well-characterized model for investigating this question. Here, we built personalized whole-brain neurophysiological models in children and adolescents to simulate task-evoked dynamics from auditory perception to language production. We demonstrate that expressive language lateralization emerges through distinct inhibitory processes. In early childhood, interhemispheric inhibitory asymmetry is present, characterized by stronger left pyramidal-to-right interneuron projections, but is insufficient to drive functional specialization. Using in silico manipulations, we show that developmental reduction in local inhibition is necessary to unmask the functional influence of early structural asymmetries. Our findings provide a mechanistic account in which expressive language specialization emerges from the interaction between early structural asymmetry and developmental disinhibition, and offer a generalizable computational framework for studying circuit specialization across species and cognitive domains.

1 Introduction

Across both natural and artificial s ystems, c omplex a nd i ntelligent behavior emerges from the coordinated interaction of simple components.[1, 2] In the brain, cognition arises from the interaction of neuronal populations organized into specialized circuits within large-scale networks.[3–5] Unlike artificial neural networks, biological networks are the product of millions of years of evolution, guided by genetic programming, and refined t hrough experience.[6, 7] T hroughout development, neural networks undergo progressive refinement, l eading t o increased specialization and localization of function, often within a single hemisphere.[8–11] Many cognitive abilities ultimately become lateralized to either the left or right hemisphere, a principle of brain organization observed across species.[12–15]

A uniquely human example of hemispheric specialization is the left hemisphere's dominant role in language processing.[11, 16–21] Language functions develop rapidly in the first y ears o f l ife, w ith m assive r estructuring o f networks supporting gross language functions in the first two decades.[22–27] D uring this period, the brain transitions from diffuse n etworks w ith r edundant connectivity to increasingly specialized and lateralized systems.[19, 20, 22, 25–28] Magnetoen-cephalography (MEG) studies have shown that the emergence of language lateralization is reflected in beta oscillatory signatures during expressive language tasks.[23, 24, 29–36] In adults, a decrease in low beta-band power (13–23 Hz), or event-related desynchronization (ERD), is observed in the left hemisphere, which reflects increased neuronal firing and metabolic demand.[24, 29, 37–40] In contrast, the right hemisphere exhibits increases in low beta-band power, or event-related synchronization (ERS), interpreted as inhibitory modulation.[23, 38–40] These beta-band dynamics, initially more bilateral in early childhood, become progressively lateralized across development.[23, 24, 41] The distributed nature of early brain networks supports plasticity in typical development and confers resilience to early brain injury.[28, 42, 43]

Despite the importance of lateralization and functional specialization to cognition across species,[8, 13, 44] we still do not understand how a diffuse and highly plastic system transitions into the physiologically efficient and specialized architecture of the adult brain.

A candidate mechanism driving the developmental transition toward specialization is the maturation of inhibitory signaling. Unlike their excitatory counterparts, inhibitory connections have a protracted postnatal development and serve as critical gatekeepers of neuroplasticity.[45–48] Previous research suggests that interhemispheric inhibition, where excitatory pyramidal neurons in one hemisphere activate inhibitory interneurons in the opposite hemisphere, supports functional lateralization.[15, 49–53] However, inhibitory interactions cannot be measured directly in the developing human brain using noninvasive methods. Computational models offer a v irtual workbench t o s imulate, p erturb, and infer physiological properties and organizational principles of brain circuits that give rise to large-scale brain activity underlying cognition.[54–58] Specifically, whole-brain networks of neural mass models allow biologically grounded simulation of macroscopic brain activity from neuronal interactions between exci-

tatory and inhibitory populations[55, 58] (see Box 1). Importantly, whole-brain models allow us to account for hierarchical dependencies between sensory processing and higher-order cognition,[59] in this case, the influence of early auditory asymmetries on later expressive language lateralization.[60]

Box 1 | Whole-brain networks of neural mass models

Neural Mass Models (NMMs) are biophysical models that describe the average activity of interacting neuronal populations (e.g., excitatory pyramidal cells and inhibitory interneurons) within a small cortical area.[61–64] By connecting multiple NMMs representing each region of the brain using the individual's connectome (structural brain connectivity typically derived from diffusion MRI in humans), we can construct whole-brain networks of neural masses (Fig. 1A).[55–58] These networks simulate activity across the brain, shaped by both local population dynamics—synaptic time constants, connection strengths, and firing rates—and long-range anatomical connections, such as pyramidal projections to inhibitory and excitatory interneurons in distant cortical regions (Fig. 1B).[65]

Neural activity simulated from each brain region approximates local field potentials and can be used to simulate signals recorded from neurophysiology or neuroimaging modalities (e.g. M/EEG and fMRI) using biophysical forward models (Fig. 1C).[66] This allows direct comparison between simulated and empirical data across one or more brain imaging modalities.[54, 67]

To allow empirical data (e.g., EEG, MEG, or fMRI) to inform model structure in the context of a research question or hypothesis, parameters can be estimated through iterative optimization to minimize the difference between simulated and observed signals (Fig. 1C).[54, 68–70]

In this study, we ask: how does the brain develop hemispheric functional specialization? This question remains central to understanding how distributed brain networks evolve into functionally asymmetric systems. We examine this question in the context of the human language system, a well-characterized model of hemispheric specialization.[22–27, 71] We hypothesize that left lateralization for expressive language is driven by the maturation of local and long-range (interhemispheric) inhibitory circuits. We predict that developmental increases in asymmetric long-range inhibitory connections in childhood drive the lateralization of beta ERD/S by adolescence. To investigate this, we constructed personalized whole-brain neurophysiological models for 43 children and adolescents (ages 4–18 years), constrained by structural connectivity derived from diffusion MRI and optimized using our machine learning approach[59, 70] to simulate MEG responses recorded during a covert expressive language task. While noninvasive imaging can reveal age-related changes in hemispheric dominance,

it cannot resolve the underlying circuit-level mechanisms. Our biophysically grounded models enable causal inference into the neural interactions that give rise to these patterns. We first assessed whether the models could reproduce a hallmark of expressive language lateralization engaged by a covert verb generation task: the developmental trajectory of beta-band (13–30 Hz) event-related desynchronization/synchronization (ERD/S).[23, 24, 29, 41] In the fitted models, we assess the strength and configuration of both local inhibitory interactions and long-range pyramidal projections, including interhemispheric pathways targeting inhibitory interneurons. In silico manipulations, including virtual circuit transplants and directional symmetrization, were then performed to test how changes in inhibition shape lateralization. Our findings reveal that functional specialization in the language system emerges as interhemispheric inhibitory pathways are developmentally unmasked through gradual reduction in local inhibition, from childhood through adolescence.

2 Results

2.1 Individual Brain Models Reproduce Auditory Evoked Responses to Linguistic and Non-Linguistic Stimuli

First, we constructed individualized whole-brain models for 43 typically developing children and adolescents (ages 4–18 years). These models simulate neural activity from auditory stimulus perception to language production. Models were constructed using individual structural connectomes derived from diffusion MRI, and optimized to fit each participant's MEG data recorded during a covert auditory verb generation task—a paradigm commonly used to assess language lateralization (Fig. 2A-B). We validated each model's simulations against the individual's empirical MEG recordings. Model parameters were optimized to reproduce the early phase (0–400 ms) of the task, capturing neural activity during auditory stimulus perception (Fig. 2B). Separate models were constructed for noun and noise trials to isolate neural responses specific to language processing. This allowed us to later compute a lateralization index based on differences in simulated beta power (13–30 Hz) during the language production window (700–1200 ms), reflecting beta-band ERD/S associated with expressive lateral-ized language activity.[23, 24, 29, 41] Model simulations successfully reproduced the timing and spatial distribution of empirical early evoked MEG activity across subjects. Figure 2C shows the model-simulated and empirical MEG time series during noun and noise trials for an exemplar subject. Across participants, model accuracy, assessed via cosine similarity between simulated and empirical MEG time series, showed consistent correspondence with empirical MEG data across subjects in both noun (mean ± SD: 0.60 ± 0.05) and noise (0.60 ± 0.05) conditions. These results validate that the models reliably reproduce neural activity during auditory stimulus perception preceding language production in this task.

2.2 Early Auditory Neural Responses Predict Lateralized Expressive Language Activity Across Age

To establish continuity between early sensory encoding and later language production, we examined whether models fit s olely t o e arly a uditory e voked responses (0–400 ms) could generalize to predict beta-band lateralization during the language production window (700–1200 ms). To do so, we simulated neural responses across the full trial duration (0–1200 ms).

We quantified b eta E RD/S l ateralization i n t he f rontal c ortex, r elevant to the task„[23, 29, 72] using a hybrid frontal laterality index (LI_{hybrid}) that contrasts left-hemisphere beta ERD and right-hemisphere beta ERS against the opposite hemispheric configuration, normalized by the total bilateral beta-band response (see Methods Section 4.9, Eq. 19).[41]

We first examined empirical b eta ERD/S p atterns. In young children (ages 5–7, n = 12), frontal beta ERD/S patterns did not differ b etween hemispheres (mean empirical LI_{hybrid} = 0.03), with no significant left–right difference in

beta power between noun and noise trials ($t(11) = 1.41$, $p > 0.05$, paired t-test, Hedge's $g = 0.43$, 95% CI $[-0.11, 0.49]$; Fig. 3A). In adolescents (ages 15–18, n = 10), empirical beta ERD/S was left-lateralized (mean $LI_{hybrid} = 0.59$), with a significant left–right difference in the noun–noise beta power difference ($t(9) = -2.36$, $p < 0.05$, paired t-test, Hedge's $g = -1.14$, 95% CI $[-0.88, -0.019]$); Fig. 3A). Across the full cohort (n = 38), empirical LI_{hybrid} significantly increased with age ($r(36) = 0.35$, $p < 0.05$, 95% CI $[0.004, 0.60]$; Fig. 3B), consistent with the developmental shift from bilateral to left-lateralized beta activity.

We then asked whether models fit solely to early auditory evoked responses (0–400 ms) could reproduce these empirical patterns of beta-band lateralization during the later language production window (700–1200 ms). Despite being optimized only on early evoked responses, the models accurately predicted beta-band lateralization. This cross-temporal generalization is notable, as models were not trained on beta-band power nor on time windows associated with lateralized beta ERD/S activity.

In young children, simulated frontal beta ERD/S patterns did not differ between hemispheres, with no significant left–right difference in beta power between noun and noise trials ($t(11) = 0.1$, $p > 0.05$, paired t-test, Hedge's $g = 0.03$, 95% CI $[-0.33, 0.36]$; Fig. 3A). The mean simulated LI_{hybrid} was 0.07, consistent with the bilateral pattern observed in the empirical data. In contrast, adolescent models exhibited left-lateralization, with a significant left–right difference in the noun–noise beta power ($t(9) = -3.74$, $p < 0.05$, paired t-test, Hedge's $g = -1.25$, 95% CI $[-0.79, -0.19]$; Fig. 3A & Fig. S1). The simulated LI_{hybrid} was 0.31, consistent with the direction of lateralization observed empirically. Across the full cohort, simulated LI_{hybrid} values also increased significantly with age ($r(36) = 0.33$, $p < 0.05$, 95% CI $[0.01, 0.59]$; Fig. 3B), closely replicating the age-related increase observed empirically.

Importantly, these models were fit solely to early evoked responses, before lateralized beta-band activity emerges, yet they successfully predict later individual differences in beta ERD/S. These results suggest that early time-locked responses encode circuit-level properties that shape subsequent oscillatory dynamics during language production, consistent with a hierarchical dependence from early sensory encoding to higher-order functional specialization within the context of a language production task. This sets the foundation for using these models to test mechanistic hypotheses about the developmental transition from bilateral to lateralized network architecture.

2.3 Inhibitory Circuit Engagement Varies with Age, Task Condition, and Lateralization

After validating that individualized brain models capture the developmental shift in expressive language lateralization, we next examined the circuit-level mechanisms associated with this transition. From each individual model, we analyzed two classes of connections: (1) local connections within each brain region, specifically, i nhibitory i nterneurons t o pyramidal c ells, pyramidal c ells t o excitatory interneurons, excitatory interneurons to pyramidal cells, and pyramidal

cells to inhibitory interneurons; and (2) interhemispheric connections between left and right frontal cortices, including pyramidal-to-pyramidal, pyramidal-to-excitatory, and pyramidal-to-inhibitory pathways. We focused on frontal regions given their established role in expressive language function and the localization of beta-band ERD/S during verb generation tasks.[23, 29, 72] Based on prior evidence linking interhemispheric inhibition to functional lateralization,[49, 51, 52, 73] we hypothesized that changes in both local and interhemispheric inhibitory connections (Fig. 4A-B) are associated with lateralization from childhood to adolescence. Among local connection types, only connections from inhibitory interneurons to pyramidal populations, reflecting local inhibition, showed a significant negative correlation with age during noun trials only ($r(36) = -0.53$, $p < 0.05$, 95% CI [−0.72, −0.25]; Fig. 4C). However, after controlling for age, which is strongly associated with language lateralization,[22] local inhibition was not significantly associated with language lateralization (semi-partial $r(36) = 0.02$, $p > 0.05$, 95% CI [−0.30, 0.34]), suggesting that the observed decline reflects a developmental trend rather than a direct driver of hemispheric dominance. In contrast, all three interhemispheric connection types significantly increased with age (Fig. 4D (pyramidal to inhibitory interneurons) $r(37) = 0.32$, $p< 0.05$, 95% CI [0.003, 0.58]; Fig. S2A (pyramidal to excitatory interneurons): $r(37) = 0.32$, $p< 0.05$,95% CI [0.005, 0.58]; Fig. S2B (pyramidal to pyramidal cells): $r(37) = 0.44$, $p < 0.05$, 95% CI [0.14, 0.66]). Only interhemispheric inhibition remained significantly a ssociated w ith l anguage l ateralization a fter controlling for age (semi-partial $r(37) = 0.37$, $p< 0.05$, 95% CI [0.063, 0.62] ; Fig. 4E). This association was specific to noun trials, suggesting that recruitment of interhemi-spheric inhibition is task-dependent and language-specific (Fig. S 2). To test the hypothesis that the dominant hemisphere exerts greater inhibitory control over its homologue, we examined the directional asymmetry of interhemispheric inhibition.[49, 51, 52, 73] We compared the strength of left-to-right (L2R) and right-to-left (R2L) pyramidal projections to inhibitory interneurons during noun trials. In both young children (4–7 years; n=12) and adolescents (15-18 years; n=10), L2R inhibition was consistently stronger than R2L inhibition (young children: two-sided paired *t*-test, $t(11) = 5.81$, $p < 0.05$, Hedge's $g = 1.69$, 95% CI [0.0008, 0.002]; adolescents: two-sided paired *t*-test, $t(9) = 4.89$, $p < 0.05$, Hedge's $g = 0.80$, 95% CI [0.0003, 0.0009]; Fig. 4F). These findings are consistent with the hypothesis that the dominant hemisphere exerts greater inhibitory control over its homologue. Between-group comparisons revealed that adolescents exhibited significantly stronger R2L inhibition than young children (independent t-test, $t(14.1) = -2.40$, $p < 0.05$, Hedge's $g = -1.03$; Fig. 4F), while L2R inhibition did not differ significantly between groups (Welch's two-sided independent t-test, $t(20.0) = -0.20$, $p = 0.844$, Hedge's $g = -0.08$). Together, these findings suggest that interhemispheric inhibitory asymmetry is established early in childhood and the mean strength of interhemispheric inhibition increases with age and predicts the degree of expressive language lateralization.

2.4 Interhemispheric Inhibition is Necessary but Not Sufficient to Induce Lateralization In Silico

Since interhemispheric inhibition during noun trials was significantly associated with beta ERD/S lateralization, we hypothesized that strengthening interhemi-spheric inhibitory connections in young children would induce lateralization, while weakening them in adolescents would disrupt it. Rather than scaling individual connections, an approach that would disregard structured patterns observed within each age group, we performed virtual transplants. For each participant, we replaced each subject's frontal interhemispheric inhibitory connections in the noun trial model with the group-average of the same connections from the other age group. All other model parameters were kept unchanged. We then re-simulated neural activity to assess whether these manipulations altered beta-band lateralization. This approach allowed us to assess the necessity of average interhemispheric inhibition for lateralization within the modeling framework. In young children, transplanting adolescent-strength interhemispheric inhibition did not induce lateralization. The lateralization index LI_{hybrid} remained unchanged at 0.07 (Fig. 5A), and beta power differences between hemispheres remained non-significant (Pre: $t(11) = 0.10$, $p > 0.05$, two-sided paired t-test, Hedge's $g = 0.03$, 95% CI $[-0.33, 0.36]$; Post: $t(11) = -0.07$, $p > 0.05$, two-sided paired t-test, Hedge's $g = 0.03$, 95% CI [-0.45, 0.42]). In contrast, transplanting child-strength interhemispheric inhibition into adolescent models disrupted lateralization, with LI_{hybrid} decreasing from 0.31 (left-lateralized) to 0.14 (bilateral; Fig. 5B). Before the transplant, adolescents exhibited significant hemispheric differences in beta power during noun versus noise trials (Pre: $t(9) = -3.74$, $p < 0.05$, two-sided paired t-test, Hedge's $g = -1.25$, 95% CI $[-0.79, -0.19]$), with lower beta power in noun trials compared to noise trials (ERD) in the left hemisphere and greater beta power (ERS) in the right hemisphere. After the transplant, this hemispheric difference w as n o longer significant (Post: $t(9) = -0.34$, $p > 0.05$, t wo-sided p aired t -test, H edge's $g = -0.13$, 95% CI [-0.50, 0.37]). While stronger interhemispheric inhibition is necessary to sustain lateralized beta ERD/S in adolescence, it is not sufficient to induce lateralization in younger brains. These findings suggest that interhemi-spheric inhibition likely interacts with other age-dependent circuit features to give rise to functional lateralization. Within the modeling framework, stronger interhemispheric inhibition was necessary to sustain lateralized beta ERD/S in adolescent simulations, but was not sufficient to induce lateralization when introduced into models of young children. These results indicate that the influence of interhemispheric inhibition on functional specialization interacts with other age-dependent circuit features to give rise to functional lateralization.

2.5 Local Inhibition Gates Effects of Interhemispheric Inhibition on Lateralization

Since increasing interhemispheric inhibition alone was not sufficient to induce lateralization in models of young children, we next asked whether a reduction in local inhibition might enable interhemispheric influences. Although local inhibition did not independently predict lateralization, its age-related decline reflects a change in the model's local inhibitory gain, corresponding to altered responsiveness of inhibitory populations targeted by interhemispheric pyramidal-to-inhibitory projections. This raised the possibility that local inhibition modulates the circuit's responsiveness to long-range input, and that both mechanisms interact to shape lateralization. To test this, we examined whether modulating local inhibition alone, while keeping interhemispheric inhibition constant, would be sufficient to induce beta ERD/S asymmetry within the model. In young children, we reduced local inhibition by subtracting the mean group-level difference in inhibitory strength from each individual's value, decreasing their average strength from 34.1 (pre-manipulation) to 33.5 (post-manipulation), matching levels observed in adolescents (Fig. 6A). Following this manipulation, re-simulated MEG activity showed lateralized beta ERD/S patterns in young children, with LI_{hybrid} increasing from 0.07 to 0.31 (Fig. 6B). This shift was marked by significant hemispheric differences in noun-noise beta power ($t(11) = -4.18$, $p < 0.05$, two-sided paired t-test, Hedge's $g = -1.44$, 95% CI $[-0.97, -0.30]$), characterized by stronger beta suppression (ERD) in the left hemisphere and enhancement (ERS) in the right hemisphere. In adolescents, we applied the reverse manipulation: increasing local inhibition by adding the same group-level difference to each individual's value, raising the average strength from 33.5 (pre-manipulation) to 34.1 (post-manipulation), matching levels observed in young children (Fig. 6C). Consequently, re-simulated beta ERD/S patterns became bilateral, and LI_{hybrid} decreased from 0.31 to 0.07 (Fig. 6D). The previously significant hemispheric difference in beta power was no longer significant ($t(9) = -1.47$, $p > 0.05$, two-sided paired t-test, Hedge's $g = -0.56$, 95% CI $[-0.65, 0.14]$). Within the modeling framework, a reduction in local inhibition was sufficient to induce lateralized beta ERD/S patterns in models of young children, and was necessary to maintain lateralization in adolescent simulations. However, this effect was observed in the presence of asymmetric interhemispheric inhibition, which is already present in models of young children (Fig. 4D). This suggests that local disinhibition modulates the circuit's sensitivity to directional interhemispheric input. We therefore hypothesized that local disinhibition enables lateralization only when asymmetric in-terhemispheric inhibition is available to drive the disinhibited circuit. If both low local inhibition and asymmetric interhemispheric inhibition are required, then eliminating asymmetry in a system where inhibition is already reduced (e.g., in adolescents) should disrupt lateralization. To test this, we symmetrized left-to-right and right-to-left interhemispheric inhibition in adolescent models and re-simulated MEG activity (Fig. 6E). Under these conditions, beta ERD/S patterns became bilateral, and the previously significant hemispheric difference

in beta power was no longer present ($t(9) = -0.84$, $p > 0.05$, two-sided paired t-test, Hedge's $g = -0.19$, 95% CI $[-0.3464,\ 0.1584]$; Fig. 6F). This demonstrates that the functional impact of reduced local inhibition in the model is contingent on the presence of asymmetric interhemispheric inhibitory input.

3 Discussion

Despite the ubiquity of hemispheric specialization in cognitive function across species, the mechanisms that govern when and how functional specialization emerges during development remain poorly understood. Inhibitory circuits are known to play a central role in regulating experience-dependent plasticity across sensory and cognitive systems, yet their contribution to the timing and expression of large-scale functional asymmetries in the human brain remains unclear. Here, we use whole-brain neurophysiological models of children and adolescents to interrogate inhibitory maturation as a developmental gating mechanism, using expressive language lateralization during a covert auditory verb generation task as a well-characterized case of hemispheric specialization. These inhibitory dynamics interact with other developmental processes, including age-related changes in white-matter organization that constrain large-scale network communication. Our findings d emonstrate t hat f unctional l ateralization d oes not arise solely from the presence of structural asymmetries, but from their functional unmasking, gated by the activity of local inhibitory circuits.

The role of interhemispheric inhibition in functional lateralization has been demonstrated in mature sensorimotor and visuospatial systems, where transcal-losal pyramidal neurons activate contralateral inhibitory interneurons to suppress competing activity.[51, 52, 73] Similar asymmetries have been inferred in the mature language system via MEG-based connectivity, with left frontal regions, such as Broca's area, demonstrating high information outflow.[72] However, these studies focused exclusively on mature, lateralized networks. Here, we demonstrate that interhemispheric inhibitory asymmetries are present in early childhood, prior to the emergence of functional lateralization (Fig. 4D). This likely reflects s tructural b iases e stablished p renatally o r i n e arly p ostnatal development. Despite early asymmetry, the presence of high local inhibition appears to suppress interhemispheric influences on network dynamics (Fig. 5A, 6C).

We show that the effects o f i nterhemispheric i nhibition o n lateralization are contingent on the state of local inhibition. In models of young children, when local inhibition is elevated, stronger interhemispheric inhibition (transplanted from adolescents) is insufficient to drive lateralization (F ig. 5A). Conversely, in models of adolescents, where local inhibition is reduced, lower mean interhemispheric inhibition (transplanted from children) eliminates lateralized activity (Fig. 5B). Importantly, the effects o f l ocal i nhibition a re bidirec-tional—decreasing local inhibition in children enables lateralization (Fig. 6C), while increasing it in adolescents suppresses it (Fig. 6D). These findings indicate that local inhibition functions as a developmental gate, regulating when interhemispheric asymmetries can shape functional organization. A potential

interpretation of these results is that heightened local inhibition in the frontal cortices of young children suppresses the expression of interhemispheric asymmetry in order to maintain a bilateral state that enhances network redundancy and plasticity during critical periods of language acquisition. This interpretation aligns with established models of plasticity regulation in other systems, such as the visual system, where local inhibition plays a crucial role in gating critical periods of experience-dependent reorganization.[47, 74, 75] Prior studies have proposed that during early development, heightened local inhibition may prevent premature specialization, instead promoting sensitivity to environmental inputs and experience-dependent plasticity.[47] Our results show that expressive language lateralization provides a well-characterized developmental context in which to study how general principles of inhibitory plasticity shape functional specialization.

Our results also show that both local and interhemispheric inhibitory mechanisms were selectively engaged during noun trials, but not noise trials (Fig. S2), suggesting their specificity to linguistic p rocessing. This aligns with previous research demonstrating that inhibitory neurons contribute to context-dependent modulation of cortical responses.[76, 77] Such effects are thought t o b e mediated by specific subsets of GABAergic neurons, recruited via long-range connections from other brain regions.[76, 78–80] Taken together, our findings and prior evidence suggest that both local and interhemispheric inhibitory mechanisms are dynamically engaged in functional specialization, shifting representation in response to developmental demands for plasticity and efficiency.

From a clinical perspective, this framework provides a mechanistic basis for understanding how language networks reorganize following focal unihemispheric injury or neurodegeneration.[14] By positing local inhibition as a gate on the functional expression of interhemispheric asymmetries, it suggests that individual differences in i nhibitory state m ay s hape c ompensatory r eorganization and recovery trajectories. In this view, bilateral expressive language representations may reflect a n a daptive, p lastic n etwork c onfiguration ra ther th an incomplete specialization, with implications for individualized intervention strategies.

Our results further show that models fitted to early auditory and receptive MEG evoked activity (0–400 ms) predict later induced beta-band ERD/ERS dynamics (700–1200 ms; Fig. 3). This finding highlights the power of computational modeling in capturing the hierarchical and temporally extended nature of brain network activity. This predictive relationship suggests that, within a verb generation context, lateralization is encoded in sensory, perceptual and expressive linguistic processes. Such a mechanism aligns with theories proposing con-tinuity between evoked sensory responses and induced higher-order processes, [81] a hierarchical organization in which early sensory processing primes the network for later lateralized activation. Here, this process involves the interaction between the long-range inhibitory connections and the stimulus to shape activation trajectories specific to language versus non-language c onditions. The differential engagement of networks in noun versus noise trials supports this interpretation, highlighting the role of early sensory activity in modulating later expressive-stage dynamics. However, it remains an open question whether this temporal

predictability reflects intrinsic properties of expressive language processing or task-specific anticipatory effects. For instance, awareness of an upcoming verb generation task may lead to pre-activation of expressive language-related circuits upon hearing the noun, biasing the network toward early engagement of expressive language-specific dynamics. Future studies could investigate this by disentangling task-driven anticipatory effects from the intrinsic temporal properties of expressive language processing. Overall, these findings reveal previously unrecognized temporal dependencies in expressive language processing.

A limitation of the present study is that the modeling results are derived from a single, modest-sized cross-sectional developmental cohort that combines individual structural connectivity with task-based MEG during auditory verb generation. Accordingly, differences observed between children and adolescents should be interpreted as cross-sectional age-related patterns rather than direct estimates of within-individual developmental trajectories. Future work will be needed to evaluate the generalization of these findings in independent samples as comparable datasets become available. To support such efforts, we provide the full analysis and modeling pipeline on GitHub at https://github.com/ Minarose/WBMLangBetaERDS and https://github.com/griffithslab/whobpyt, enabling replication and extension of this framework in future datasets and clinical populations.

Several avenues for future research emerge from this work. Given the cross-sectional nature of the present study, extending this framework to longitudinal designs will be essential for tracking within-individual developmental trajectories and for determining how local and interhemispheric inhibitory mechanisms interact with behavioral, environmental, and neurochemical factors to shape functional lateralization. Integrating our computational approach with direct measurements of inhibitory neurotransmitters through magnetic resonance spectroscopy could provide complementary validation of model-derived inhibitory parameters.[82] Moreover, applying our in silico modeling framework to other cognitive domains and to language tasks engaging other linguistic processes would reveal whether the developmental principles identified here represent universal mechanisms of functional hemispheric specialization. An important direction for future work will be to extend this framework to model functional connectivity in the language network, linking developmental changes in specific functional connections to the emergence of lateralized oscillatory states in these models. In addition, future work integrating tract-specific microstructural measures sensitive to axonal and myelin-related properties will be important for disentangling how white-matter maturation shapes interhemispheric communication beyond the effective coupling estimated here. Complementary studies incorporating tract-specific analyses, finer-grained regional models, and diverse language tasks will further be critical for situating this inhibitory gating mechanism within classical language pathways and dual-stream architectures. Finally, future applications of this framework to conditions characterized by atypical language development could provide mechanistic insights into underlying circuit abnormalities, potentially guiding targeted interventions. Throughout this work, causal inferences are made at the level of the computational model: the

in silico manipulations identify circuit configurations that are necessary and sufficient to reproduce observed developmental patterns within the modeling framework, and thus propose a candidate mechanistic hypothesis to be tested empirically in future experimental studies.

4 Methods

4.1 Participants

Forty-three typically developing children and adolescents (20 females; ages 4–18 years, mean age = 11.3) participated in this study. All participants were native English speakers, with no history of neurological, psychological, speech, or language impairments. Handedness was assessed using the Edinburgh Handedness Inventory (EHI),[83] computed as a laterality index ranging from -100 (strong left) to $+100$ (strong right). Across the cohort, 81% of participants were right-handed, 14% had no hand preference, and 5% were left-handed. EHI scores were not correlated with age (Spearman's $\rho = 0.096$, $p = 0.54$). Informed written consent was obtained from all participants and/or their guardians, and assent from the minor participant was documented. The study was approved by the Institutional Review Board at Cincinnati Children's Hospital Medical Center (OH, USA; data collection site) and the Research Ethics Board at the Hospital for Sick Children (Toronto, ON, Canada; data analysis site). All procedures complied with the US Federal Policy for the Protection of Human Subjects and adhered to the Declaration of Helsinki.

4.2 Empirical Data Acquisition

4.2.1 Structural MRI

The anatomical MRI scans were acquired at 3.0 T on a Philips Achieva or In-genia Elition scanner (Philips Medical Systems, International). Whole-brain 3D T1-weighted images were acquired using an MDEFT scan (flip angle = 90°, TE = 3.7 ms, TR = 8.1 ms, voxel size = 1.0 × 1.0 × 1.0 mm). Multimodal radiographic markers were placed over the nasion and preauricular points to facilitate coregistration with MEG.

4.2.2 Diffusion MRI

Diffusion-weighted MR images were acquired on the same scanner across three diffusion-encoding shells (b = 1000 s/mm^2 (45 directions), b = 2000 s/mm^2 (56 directions), and b = 3000 s/mm^2 (68 directions)), at a resolution of 2.0 × 2.0 × 2.0 mm, with interspersed b0 volumes. Additional reverse-phase encoded b0 images were acquired to enable offline geometric distortion correction.

4.2.3 MEG

MEG data were acquired using a whole-head 275-channel CTF system (MEG International Services Ltd., Coquitlam, B.C., Canada) with a sampling rate of 1.2 kHz. Participants were studied in the supine position. MEG sessions were limited to less than 30 minutes, in order to minimize fatigue and maximize participation in the studies. Stimuli were presented binaurally by an intensity calibrated distal transducer through tubing and ear inserts (Etymotic Research,

IL, USA). Head localization coils were positioned at the nasion and preauricular points to continuously monitor head movement during data acquisition. These fiducial landmarks enabled precise co-registration of MEG data with structural MRIs. Head motion was monitored throughout the recording using three head localization coils, with datasets retained only if total displacement remained below 5 mm across the acquisition. Participants completed a covert auditory verb generation task in the MEG, an expressive language task previously employed by our group.[23, 24, 41, 72] A covert design was used to minimize head movement and muscle-related artifacts associated with overt speech which can obscure oscillatory signatures, particularly in the beta band.[84] Converging M/EEG evidence indicates that covert and overt speech production elicit comparable mu- and beta-band ERD/ERS dynamics and hemispheric lateralization patterns.[85–89] Participants listened to either a noun (verb generation trials), or speech-shaped noise (control trials). During verb generation trials, they were instructed to covertly generate a single action word related to each noun, without overt speech production. Although no overt articulation was required, the task was designed to engage lexical retrieval and speech production processes up to the level of articulatory planning, rather than purely semantic association. Prior to MEG recording, participants practiced an overt version of the task to confirm t ask c omprehension a nd appropriate verb selection (at least 8/10 items correct), after which they were instructed to perform the same operation covertly during scanning. The noun stimuli consisted of familiar items (e.g., pencil, book, dog) selected from normative databases and standardized language assessments, ensuring age-appropriate familiarity for a typically developing 5-year-old. In control trials, participants listened to noise stimuli without responding. Noun and noise stimuli were presented randomly, with a jittered interstimulus interval of 4–5 seconds. In total, participants completed 71 unique noun and noise trials, each lasting 670 ms (mean ± 140 ms).

4.3 Empirical Data Pre-Processing and Analysis

4.3.1 Diffusion MRI

Preprocessing of the diffusion-weighted images (DWI) was performed using FSL and MRtrix3.[90, 91] First, the data were denoised and corrected for Gibbs ringing artifacts.[92, 93] Geometric distortions were corrected using FSL's topup tool.[94, 95] Motion and eddy-current correction were performed using FSL's eddy with slice-to-volume correction, outlier replacement, and subject-specific q uality control metrics.[96] Eddy quality control outputs were visually inspected, and no datasets were excluded beyond predefined acquisition f ailures. Bias field inhomogeneity correction was performed using the N4ITK algorithm to improve brain mask estimation and achieve intensity uniformity.[97] Response functions for white matter (WM), gray matter (GM), and cerebrospinal fluid (CSF) were estimated from multi-shell data, enabling tissue-specific fiber orientation an alysis. Voxel-wise fiber orientation distributions (FODs) were calculated using Constrained

Spherical Deconvolution (CSD), allowing robust estimation of crossing fibers.[98] Global intensity normalization was applied to the FOD images to minimize intensity variations across scans. Anatomically constrained tractography was employed to generate 10 million streamlines originating and terminating at the gray-white matter junction using second-order integration over fiber orientation distributions.[99] To further improve the quantitative accuracy of the connectivity representation, spherical-deconvolution informed filtering o f tractograms (SIFT2) was applied.[100] SIFT2 assigns weights to streamlines to ensure that streamline densities are proportional to the underlying fiber p opulation densities represented by the FOD.[100] Finally, anatomical connectivity weight matrices were derived based on the number of streamlines between regions parcellated using the 184-region Shen atlas.[101]

4.3.2 MEG

MEG data were preprocessed and analyzed using FieldTrip[102] in MATLAB R2020b (MathWorks Inc., Natick, MA, USA). Data were segmented into epochs spanning -500 to 1500 ms relative to stimulus onset for both verb generation and control trials. Line noise at 60 Hz and its harmonics (120 Hz, 180 Hz) was attenuated with a sharp discrete Fourier transform filter, followed by bandpass filtering f rom 2 t o 4 0 H z. T he d ata w ere t hen d ownsampled t o 1 000 H z to match the sampling rate of the simulated time series. Independent Component Analysis (ICA) with 20 components was performed using the InfoMax algorithm. Stereotypical blink and cardiac artifacts were identified visually from component topographies and time series, then removed. Trials were demeaned, and SQUID jump artifacts were automatically detected. Trials with jump artifacts (mean ± SD = 1.68 ± 1.16, range = 0–4) were excluded. For model parameter fitting, trials were cropped to -100 to 400 ms post-stimulus and averaged to create a single evoked time series in sensor space for each condition (see Model Fitting & Parameter Estimation).

To compare empirical and simulated source activity, MEG source reconstruction was performed on the entire epoch. Covariance matrices were computed from concatenated noun and noise trials for each participant. Realistic single-shell head models were constructed from the brain surface extracted from the segmented T1 images.[103] A whole-brain source model was created based on the centroids of the 184-region Shen atlas,[101] warped to individual space using non-linear transformations to account for anatomical variability. This approach localized 184 sources, across the cerebrum and cerebelli. Source time series from 184 regions were estimated using the individual source models and a linearly constrained minimum variance (LCMV) beamformer with 1% regularization.

4.4 Computational Brain Network Models

Each network consisted of 184 nodes, based on the Shen atlas regions, connected by weights derived from the individual's anatomical connectivity matrix (see Diffusion MRI section). Regional brain dynamics were modeled in each node

using Jansen-Rit (JR) neural mass model[63] that simulates the macroscopic elec-trophysiological activity within a cortical column. This model has been extensively validated for reproducing a wide range of M/EEG oscillation frequencies and evoked response waveforms.[63, 64, 70, 104] It consists of three interconnected neural populations: pyramidal cells found in agranular layers, excitatory in-terneurons predominantly in the granular layer, and inhibitory interneurons found in the agranular layers.[63, 64] These populations are connected in excitatory and inhibitory loops. The inhibitory loop consists of connections from (i) pyramidal cells to inhibitory interneurons, and (ii) inhibitory interneurons to pyramidal cells. The excitatory loop consists of connections from (i) pyramidal to excitatory interneurons, and (ii) excitatory interneurons to pyramidal cells. Each node has three types of long-range extrinsic connections originating from the pyramidal cells, based on the Felleman & Van Essen rules.[105] Connections from pyramidal cells to inhibitory and excitatory interneurons are directed, while connections from pyramidal to pyramidal cells are undirected. Within each of the three neural populations, the post-synaptic somatic and dendritic membrane response to incoming action potentials is described by second-order differential equations:

$$\ddot{v}(t) + \frac{2}{\tau}\dot{v}(t) + \frac{1}{\tau^2}v(t) = \frac{H}{\tau}m(t) \tag{1}$$

where v is the postsynaptic membrane potential, H is the maximum postsy-naptic potential, τ is a lumped representation of delays occurring during the synaptic transmission, and m is the (population-average) presynaptic input. This equation is equivalent to convolving the incoming activity with a synaptic impulse response function, often referred to as a pulse-to-wave operator:

$$v(t) = \int_0^\infty d\tau\, m(\tau) \cdot h(t-\tau) \tag{2}$$

The kernel h(t) of this function is given by:

$$h = \frac{H}{\tau} \cdot t \cdot \exp\left(-\frac{t}{\tau}\right) \tag{3}$$

Each neural population incorporates a wave-to-pulse operator that converts the somatic membrane potential into the population's output firing rate using a sigmoid function, represented as:

$$S(v) = \frac{e_0}{1 + \exp(r(v_0 - v))} \tag{4}$$

where e_0 is the maximum firing r ate, r i s t he s igmoid f unction's steepness, and v_0 is the postsynaptic potential at which half the maximum firing r ate is achieved. Together, the complete JR model for each cortical area j in a network of N regions is expressed as three sets of second-order differential equations that follow the structure of Equation 1, extended into three sets of coupled first-order

ARTICLE IN PRESS

differential equations:

$$\dot{v}_{j1} = x_{j1} \tag{5}$$

$$\dot{x}_{j1} = \frac{H_e}{\tau_e}\left[C_1 S\left(C_2 v_{j3}\right) + g_{pe} I_{pe\,j}\right] - \frac{2}{\tau_e} x_{j1} - \frac{1}{\tau_e^2} v_{j1} \tag{6}$$

$$\dot{v}_{j2} = x_{j2} \tag{7}$$

$$\dot{x}_{j2} = \frac{H_i}{\tau_i}\left[C_4 S\left(C_3 v_{j3}\right) + g_{pi} I_{pi\,j}\right] - \frac{2}{\tau_i} x_{j2} - \frac{1}{\tau_i^2} v_{j2} \tag{8}$$

$$\dot{v}_{j3} = x_{j3} \tag{9}$$

$$\dot{x}_{j3} = \frac{H_e}{\tau_e}\left[S\left(v_{j1} - v_{j2}\right) + g_{pp} I_{pp\,j} + p_j\right] - \frac{2}{\tau_e} x_{j3} - \frac{1}{\tau_e^2} v_{j3} \tag{10}$$

where $v_{j1,2,3}$ is the average postsynaptic membrane potential and $x_{j\,1,2,3}$ are the mean currents of the excitatory interneuron, inhibitory interneuron, and pyramidal cell populations, respectively. Here, g denotes the global coupling strength between pyramidal cells and excitatory interneurons (g_{pe}), pyramidal cells and inhibitory interneurons (g_{pi}), pyramidal and pyramidal cells (g_{pp}). C represents the local coupling strengths between neuronal populations. Specifically, C_1 denotes the coupling from the pyramidal population to the excitatory interneuron, C_2 from the excitatory interneuron to the pyramidal population, C_3 from the pyramidal population to the inhibitory interneuron, and C_4 from the inhibitory interneuron to the pyramidal population. The input from other ,I_{jpe} ,I_{jpi}:nodes, j, in the whole-brain network is modeled by I_{jpp}

$$I_{pp\,j} = \sum_{i=1}^{N} W_{pp\,ij}\left(v_{i3} - v_{j3}\right) \tag{11}$$

$$I_{pe\,j} = \sum_{i=1}^{N} W_{pe\,ij}\left(v_{i3} - v_{j3}\right) \tag{12}$$

$$I_{pi\,j} = \sum_{i=1}^{N} W_{pi\,ij}\left(v_{i3} - v_{j3}\right) \tag{13}$$

Here, W_{ijpp} refers to the element in the i_{th} row and j_{th} column of the connectivity matrix, between pyramidal populations (pp) , W_{ijpe} corresponds to the same element in the directed connectivity matrix between pyramidal populations and excitatory interneurons (pe), and $W_{ij\,pi}$ represents the corresponding element in the directed connectivity matrix between pyramidal populations and inhibitory interneurons (pi). Due to the finite velocity of long-range axonal conduction, these inputs experience delays ranging from approximately 5 to 50 ms, depending on the physical length of each connection. These temporal delays are represented by m_{ij}, the i,j -th entry in the delay matrix M, calculated as T/s. Here, T is the inter-regional fiber tract length matrix, and s is the global axonal conduction velocity. We simulated stimulus-evoked depolarization of the resting membrane potential by applying an external perturbing voltage offset,

p_j, specifically targeting the pyramidal population to reflect the influence of external inputs. Sensor space MEG activity was simulated by computing the difference between the excitatory $v_1(t)$ and inhibitory $v_2(t)$ interneuron post-synaptic potentials, representing the net somatic membrane potential of the pyramidal cell population, at each cortical region and projecting these signals into sensor space using Maxwell's equations as the forward solution:

$$Y = G \bullet X + \epsilon \tag{14}$$

where Y represents the MEG sensor data, G is the participant-specific leadfield matrix, X is the source activity at cortical regions, and ϵ accounts for measurement noise and model inaccuracies. The leadfield matrix G was computed individually for each participant using FieldTrip accounting for each participant's head geometry and sensor layout.

4.5 Model Fitting & Parameter Estimation Using MEG Data

We utilized a machine learning-based parameter estimation approach, Whole-Brain Modelling in PyTorch (WhoBPyt), to fit individual brain network models.[70] In this paper, we fitted two models for each individual with the early MEG activity (0-400 ms post-stimulus) averaged across noun and noise trials. Models were fitted to minimize the mean-squared error term in sensor space comparing simulated and empirical MEG time series. Simulated time series were generated using the same individual source models estimated for the empirical source modelling. Trial-averaged MEG evoked responses were divided into short 50 ms non-overlapping windows, termed batches. We introduced a noise input term to all neural populations to account for background neural activity and improve model robustness. The total length of the simulation was 500 ms which included −100 ms of baseline (pre-stimulus) and +400 ms after stimulation injection. We sequentially processed each batch of the time series to simulate evoked activity $\hat{y}$ using the Jansen-Rit (JR) model and forward-Euler integration of the model equations 1-6. Difference between the simulated evoked activity $\hat{y}$ the empirical activity y was evaluated using the mean-squared error (MSE) loss function:

$$L = \frac{1}{N_t} \sum_{t=1}^{N_t} \frac{1}{N_{\text{sens}}} \sum_{i=1}^{N_{\text{sens}}} (y_i(t) - \hat{y}_i(t))^2 \tag{15}$$

where N_t is the number of time points, N_{sens} is the number of MEG sensors, $y_i(t)$ is the observed value at time t for sensor i, $\hat{y}_i(t)$ is the simulated value, and L represents the total loss.

To prevent overfitting and enhance robustness, a complexity-penalizing regularization term C incorporating Gaussian priors was added for each model parameter θ:

$$C = \ln \sigma + \frac{1}{\sigma^2} (\theta - \mu)^2 \tag{16}$$

ARTICLE IN PRESS

where the mean μ and standard deviation σ of the model parameter θ serve as optimization hyperparameters. The loss function L and the complexity term C are combined into a final objective function O:

$$O = L + \lambda C \tag{17}$$

which balances the data loss and the regularization term through a parameter λ. The objective function was optimized using PyTorch's ADAM algorithm.[106] The optimization iterated over batches of the time series until convergence. Parameters were allowed to vary per subject under tight constraints with low-variance priors. The last 100 batches were then used to compute the average value for each parameter which was used for subsequent simulations. In this work, these parameter values were used to simulate 1200 ms of activity.

To simulate the auditory verb generation task, we modeled the auditory stimulus as a 40 ms square-wave input injected bilaterally into neural masses representing left and right Heschl's gyri. These nodes were identified using an ROI mask of left and right Heschl's gyri based on the Talairach Daemon database.[107]

4.6 Goodness of Fit

To inspect the goodness-of-fit of the optimized MEG evoked fields, we quantified cosine similarity between empirical and simulated time series averaged across sensors for each participant.

$$\text{Cosine Similarity} = \frac{\mathbf{x}\cdot\mathbf{y}}{||\mathbf{x}||||\mathbf{y}||} = \frac{\sum_{i=1}^{n} x_i y_i}{\sqrt{\sum_{i=1}^{n} x_i^2}\sqrt{\sum_{i=1}^{n} y_i^2}} \tag{18}$$

Here, x and y represent the empirical and simulated time series, respectively, and n is the number of time points. A cosine similarity value close to 1 indicates high similarity, whereas values closer to 0 suggest low alignment.

4.7 Task-Related Beta ERD/ERS Quantification

For the empirical MEG data, task-related beta-band event-related desynchro-nization and synchronization (ERD/ERS) were quantified at each cortical dipole position by contrasting noun and noise conditions. Power spectral density estimates were computed for individual trials in the beta band (13–30 Hz) within the 700–1200 ms post-stimulus window. For each dipole, t-statistics were computed comparing beta power between noun and noise trials. Statistical significance was assessed using nonparametric permutation testing (Monte Carlo simulation in FieldTrip),[102] in which condition labels were randomly shuffled ac ross trials (10,000 permutations; $\alpha = 0.05$). Dipoles exhibiting statistically significant task-related beta modulation were defined a s s uprathreshold a nd r etained for subsequent analyses. Negative t-values were interpreted as event-related desyn-chronization (ERD), reflecting decreased beta power during noun trials relative to noise, whereas positive t-values were interpreted as event-related synchronization (ERS).

4.8 Model Beta ERD/S Prediction

Whole-brain model simulations of both noun and noise conditions were extended to 1200 ms post-stimulus. Beta power (13–30 Hz) was computed using Welch's method within the same 700–1200 ms time window, and model-predicted beta ERD/S was defined as the difference in beta power between noun and noise simulations. Model-derived beta ERD/S values were extracted only from the frontal regions identified as suprathreshold in the empirical analysis.

4.9 Beta ERD/S Hybrid Laterality Index

Hemispheric lateralization of task-related beta responses was quantified using a hybrid ERD/S laterality index[41] which captures the asymmetric distribution of beta ERD/ERS across hemispheres:

$$LI_{\text{hybrid}} = \frac{(ERD_L + ERS_R) - (ERD_R + ERS_L)}{(ERD_L + ERS_R) + (ERD_R + ERS_L)} \tag{19}$$

where $\mathrm{ERD_L}$ and $\mathrm{ERD_R}$ are the beta-band event-related desynchronization in the left and right hemispheres, and $\mathrm{ERS_L}$ and $\mathrm{ERS_R}$ refer to the beta-band event-related synchronization in the left and right hemispheres, respectively. Scores range from −1 to + 1, with −1 indicating right lateralization of ERD, and + 1 indicating left lateralization of ERD. Predicted LIs from the model were compared to empirically observed LIs using Pearson correlations and linear regression. Subjects with no empirical suprathreshold ERD/S were excluded from further analyses (n=5).

4.10 Statistical Analyses

All statistical analyses were performed using Python (version 3.8) with the SciPy (version 1.7) and StatsModels (version 0.13) libraries. Outliers were identified as values outside $Q_1 - 1.5 \times \mathrm{IQR}$ and $Q_3 + 1.5 \times \mathrm{IQR}$, where Q_1 and Q_3 are the 25th and 75th percentiles, respectively. Pearson correlation analyses were conducted to examine the relationships between parameters and age, with significance set at $p < 0.05$. For the relationship b etween parameters and LI_{hybrid}, residuals were calculated by regressing out age, enabling an age-independent analysis using Pearson correlations. Additionally, multiple regression analyses were employed to account for potential confounding effects of age and other connection types. Paired t-tests were used to compare left-to-right (L2R) versus right-to-left (R2L) coupling strength differences w ithin g roups a nd noun-noise beta power differences b etween l eft a nd r ight f rontal r egions. I ndependent t-tests were employed to compare mean coupling strengths between groups and to assess differences in L2R and R2L values across groups.

4.11 Virtual P-I Transplant Experiments

To test the causal role of interhemispheric pyramidal to inhibitory connections in expressive language lateralization, we performed virtual transplant experiments.

We replaced the frontal interhemispheric P-I connection weights of individuals from one group (e.g., adolescents) with the mean P-I connection weights from another group (e.g. young children). Brain activity was then re-simulated using these modified connectomes, and changes in lateralization patterns were quantified.

4.12 Local I to P Manipulation

The local I-to-P coupling strength for each subject was adjusted by either subtracting or adding the mean difference in coupling strength observed between groups. Brain activity was then re-simulated, and the resulting changes in lateralization patterns were quantified.

4.13 Interhemispheric P-I Symmetrization

To symmetrize interhemispheric inhibition in adolescent models, all right-to-left (R2L) frontal pyramidal-to-inhibitory (P–I) connection values were set equal to their corresponding left-to-right (L2R) values, effectively removing directional asymmetry. All other model parameters were held constant. Brain activity was then re-simulated using the symmetrized connectomes to assess the effect of eliminating interhemispheric inhibition asymmetry on lateralization.

Data Availability

The preprocessed data used in this study are publicly available on GitHub at https://github.com/Minarose/WBMLangBetaERDS and https://github.com/griffithslab/whobpyt. Due to institutional privacy restrictions, raw imaging data cannot be hosted directly in these repositories but will be made available to qualified r esearchers u pon r easonable r equest, i n a ccordance with institutional ethics requirements and data protection policies.

Code Availability

The code required to reproduce the analyses, model parameters, and figures is publicly available at
https://github.com/Minarose/WBMLangBetaERDS and
https://github.com/griffithslab/whobpyt.

5 Acknowledgments

This study was supported by the National Institute of Neurological Disorders and Stroke (NINDS) at the National Institutes of Health (NIH), under award R21NS106631 (D.S.K./H.M.G.). The content is solely the responsibility of the authors and does not necessarily represent the official vi ews of th e NI H. Data collection was conducted at Cincinnati Children's Hospital Medical Center, and analysis was performed at the Hospital for Sick Children (Toronto), in strict compliance with institutional ethical guidelines.

6 Author Contributions

M.M.I.: Conceptualization, Methodology, Software, Formal analysis, Investigation, Data Curation, Writing - Original Draft, Writing - Review & Editing, Visualization. **D.M. and Z.W.**: Conceptualization, Methodology, Software, Writing - Original Draft, Writing - Review & Editing. **S.P.B. and M.P.O.**: Methodology, Software, Writing - Review & Editing. **H.M.G.**: Resources, Writing - Review & Editing, Funding acquisition. **D.J.M.**: Conceptualization, Writing - Review & Editing. **J.D.G.**: Conceptualization, Methodology, Software, Writing - Review & Editing, Supervision, Resources. **D.S.K.**: Conceptualization, Methodology, Software, Writing - Review & Editing, Supervision, Resources, Funding acquisition.

7 Competing Interests

The authors declare no competing interests.

References

[1] Olaf Sporns. From complex networks to intelligent systems. In Creating brain-like intelligence: From basic principles to complex intelligent systems, pages 15–30. Springer, 2009.

[2] Mikail Khona, Sarthak Chandra, and Ila Fiete. Global modules robustly emerge from local interactions and smooth gradients. Nature, pages 1–10, 2025.

[3] Steven L Bressler and Vinod Menon. Large-scale brain networks in cognition: emerging methods and principles. Trends in cognitive sciences, 14(6):277–290, 2010.

[4] Anthony Randal McIntosh. Towards a network theory of cognition. Neural networks, 13(8-9):861–870, 2000.

[5] Hae-Jeong Park and Karl Friston. Structural and functional brain networks: from connections to cognition. Science, 342(6158):1238411, 2013.

[6] Liqun Luo. Architectures of neuronal circuits. Science, 373(6559):eabg7285, 2021.

[7] Onur Güntürkün and Sebastian Ocklenburg. Ontogenesis of lateralization. Neuron, 94(2):249–263, 2017.

[8] Gesa Hartwigsen, Yoshua Bengio, and Danilo Bzdok. How does hemispheric specialization contribute to human-defining cognition? Neuron, 109(13):2075–2090, 2021.

[9] Miguel L Concha, Isaac H Bianco, and Stephen W Wilson. Encoding asymmetry within neural circuits. Nature Reviews Neuroscience, 13(12):832–843, 2012.

[10] Liliann Manning and Catherine Thomas-Antérion. Marc dax and the discovery of the lateralisation of language in the left cerebral hemisphere. Revue neurologique, 167(12):868–872, 2011.

[11] Paul Broca et al. Remarks on the seat of the faculty of articulated language, following an observation of aphemia (loss of speech). Bulletin de la Société Anatomique, 6(330-357):27, 1861.

[12] Arthur W Toga and Paul M Thompson. Mapping brain asymmetry. Nature Reviews Neuroscience, 4(1):37–48, 2003.

[13] Onur Güntürkün, Felix Ströckens, and Sebastian Ocklenburg. Brain lateralization: a comparative perspective. Physiological reviews, 2020.

[14] Sebastian Ocklenburg, Annakarina Mundorf, Robin Gerrits, Emma M Karlsson, Marietta Papadatou-Pastou, and Guy Vingerhoets. Clinical implications of brain asymmetries. Nature Reviews Neurology, 20(7):383– 394, 2024.

[15] Vyacheslav R Karolis, Maurizio Corbetta, and Michel Thiebaut de Schot-ten. The architecture of functional lateralisation and its relationship to cal-losal connectivity in the human brain. Nature communications, 10(1):1417, 2019.

[16] Carl Wernicke. Der aphasische symptomencomplex. Die Deutsche Klinik, 6:487–556, 1903.

[17] RR Benson, DB FitzGerald, LL LeSueur, DN Kennedy, KK Kwong, BR Buchbinder, TL Davis, RM Weisskoff, TM Talavage, WJ Logan, et al. Language dominance determined by whole brain functional mri in patients with brain lesions. Neurology, 52(4):798–798, 1999.

[18] Jeffrey R Binder, Stephen M Rao, Thomas A Hammeke, Julie A Frost, Peter A Bandettini, Andrzej Jesmanowicz, and James S Hyde. Lateralized human brain language systems demonstrated by task subtraction functional magnetic resonance imaging. Archives of Neurology, 52(6):593–601, 1995.

[19] Norman Geschwind. The organization of language and the brain: Language disorders after brain damage help in elucidating the neural basis of verbal behavior. Science, 170(3961):940–944, 1970.

[20] Cathy J Price. A review and synthesis of the first 20 years of pet and fmri studies of heard speech, spoken language and reading. Neuroimage, 62(2):816–847, 2012.

[21] Loïc Labache, Tian Ge, BT Thomas Yeo, and Avram J Holmes. Language network lateralization is reflected throughout the macroscale functional organization of cortex. Nature communications, 14(1):3405, 2023.

[22] Jerzy P Szaflarski, Jeffrey R Binder, Edward T Possing, Kristen A McK-iernan, B Douglas Ward, and Thomas A Hammeke. Language lateralization in left-handed and ambidextrous people: fmri data. Neurology, 59(2):238–244, 2002.

[23] Vivek V Sharma, Jennifer Vannest, Hansel M Greiner, Hisako Fujiwara, Jeffrey R Tenney, Brady J Williamson, and Darren S Kadis. Beta synchrony for expressive language lateralizes to right hemisphere in development. Scientific reports, 11(1):3949, 2021.

[24] Darren S Kadis, Elizabeth W Pang, Travis Mills, Margot J Taylor, Mary Pat McAndrews, and Mary Lou Smith. Characterizing the normal developmental trajectory of expressive language lateralization using magnetoencephalography. Journal of the International Neuropsychological Society, 17(5):896–904, 2011.

[25] Scott K Holland, Jennifer Vannest, Marc Mecoli, Lisa M Jacola, Jan-Mendelt Tillema, Prasanna R Karunanayaka, Vincent J Schmithorst, Wei-hong Yuan, Elena Plante, and Anna W Byars. Functional mri of language

lateralization during development in children. International journal of audiology, 46(9):533–551, 2007.

[26] Jerzy P Szaflarski, Vincent J Schmithorst, Mekibib Altaye, Anna W Byars, Jennifer Ret, Elena Plante, and Scott K Holland. A longitudinal functional magnetic resonance imaging study of language development in children 5 to 11 years old. Annals of Neurology: Official Journal of the American Neurological Association and the Child Neurology Society, 59(5):796–807, 2006.

[27] Angela D Friederici. The brain basis of language processing: from structure to function. Physiological reviews, 91(4):1357–1392, 2011.

[28] Brady J Williamson, Hansel M Greiner, and Darren S Kadis. Virtual lesions in meg reveal increasing vulnerability of the language network from early childhood through adolescence. Nature Communications, 14(1):7313, 2023.

[29] Elizabeth W Pang, Frank Wang, Marion Malone, Darren S Kadis, and Elizabeth J Donner. Localization of broca's area using verb generation tasks in the meg: Validation against fmri. Neuroscience letters, 490(3):215–219, 2011.

[30] Vahab Youssofzadeh, Jeffrey Stout, Candida Ustine, William L Gross, Lisa L Conant, Colin J Humphries, Jeffrey R Binder, and Manoj Ragha-van. Mapping language from meg beta power modulations during auditory and visual naming. NeuroImage, 220:117090, 2020.

[31] Kirsten Herfurth, Yuval Harpaz, Julie Roesch, Nadine Mueller, Katrin Walther, Martin Kaltenhaeuser, Elisabeth Pauli, Abraham Goldstein, Hajo Hamer, Michael Buchfelder, et al. Localization of beta power decrease as measure for lateralization in pre-surgical language mapping with magnetoencephalography, compared with functional magnetic resonance imaging and validated by wada test. Frontiers in Human Neuroscience, 16:996989, 2022.

[32] Anne M Findlay, Josiah B Ambrose, Deborah A Cahn-Weiner, John F Houde, Susanne Honma, Leighton BN Hinkley, Mitchel S Berger, Srikan-tan S Nagarajan, and Heidi E Kirsch. Dynamics of hemispheric dominance for language assessed by magnetoencephalographic imaging. Annals of neurology, 71(5):668–686, 2012.

[33] Alison Eleanor Fisher, Paul Lawrence Furlong, Stefano Seri, Peyman Adjamian, Caroline Witton, Torsten Baldeweg, Sunny Phillips, Richard Walsh, Judith M Houghton, and Ngoc Jade Thai. Interhemispheric differences of spectral power in expressive language: a meg study with clinical applications. International journal of psychophysiology, 68(2):111–122, 2008.

[34] Volker Ressel, Marko Wilke, Karen Lidzba, Werner Lutzenberger, and Ingeborg Krägeloh-Mann. Increases in language lateralization in normal children as observed using magnetoencephalography. Brain and language, 106(3):167–176, 2008.

[35] Sabine Weiss and Horst M Mueller. "too many betas do not spoil the broth": the role of beta brain oscillations in language processing. Frontiers in psychology, 3:201, 2012.

[36] Masayuki Hirata, Amami Kato, Masaaki Taniguchi, Youichi Saitoh, Hiro-tomo Ninomiya, Aya Ihara, Haruhiko Kishima, Satoru Oshino, Takahito Baba, Shiro Yorifuji, et al. Determination of language dominance with synthetic aperture magnetometry: comparison with the wada test. Neu-roimage, 23(1):46–53, 2004.

[37] Christa Neuper, Michael Wörtz, and Gert Pfurtscheller. Erd/ers patterns reflecting sensorimotor activation and deactivation. Progress in brain research, 159:211–222, 2006.

[38] G Pfurtscheller. Eeg rhythms-event-related desynchronization and synchronization. In Rhythms in Physiological Systems: Proceedings of the International Symposium at Schlo Elmau, Bavaria, October 22–25, 1990, pages 289–296. Springer, 1991.

[39] Gert Pfurtscheller. Event-related synchronization (ers): an electrophys-iological correlate of cortical areas at rest. Electroencephalography and clinical neurophysiology, 83(1):62–69, 1992.

[40] Gert Pfurtscheller, Clemens Brunner, Alois Schlögl, and FH Lopes Da Silva. Mu rhythm (de) synchronization and eeg single-trial classification of different motor imagery tasks. NeuroImage, 31(1):153–159, 2006.

[41] Vivek V Sharma and Darren S Kadis. A powerful metric for expressive language lateralization in meg. Neuroscience Letters, 818:137539, 2024.

[42] Keith R Thulborn, Patricia A Carpenter, and Marcel A Just. Plasticity of language-related brain function during recovery from stroke. Stroke, 30(4):749–754, 1999.

[43] M Esteves, E Ganz, N Sousa, and H Leite-Almeida. Asymmetrical brain plasticity: physiology and pathology. Neuroscience, 454:3–14, 2021.

[44] Sebastian Ocklenburg and Onur Güntürkün. Hemispheric asymmetries: the comparative view. Frontiers in psychology, 3:5, 2012.

[45] BERND SUTOR and HEIKO J LUHMANN. Development of excitatory and inhibitory. Perspectives on developmental neurobiology, 2(43):409– 419, 1995.

[46] Dimitri M Kullmann, Alexandre W Moreau, Yamina Bakiri, and Elizabeth Nicholson. Plasticity of inhibition. Neuron, 75(6):951–962, 2012.

[47] Taro Toyoizumi, Hiroyuki Miyamoto, Yoko Yazaki-Sugiyama, Nafiseh At-apour, Takao K Hensch, and Kenneth D Miller. A theory of the transition to critical period plasticity: inhibition selectively suppresses spontaneous activity. Neuron, 80(1):51–63, 2013.

[48] Takao K Hensch. Critical period plasticity in local cortical circuits. Nature reviews neuroscience, 6(11):877–888, 2005.

[49] J Netz, U Ziemann, and V Hömberg. Hemispheric asymmetry of transcal-losalinhibition in man. Experimental brain research, 104:527–533, 1995.

[50] Michael S Gazzaniga. Forty-five years of split-brain research and still going strong. Nature Reviews Neuroscience, 6(8):653–659, 2005.

[51] Anna L Mangia, Mauro Ursino, Maurizio Lannocca, and Angelo Cappello. Transcallosal inhibition during motor imagery: Analysis of a neural mass model. Frontiers in computational neuroscience, 11:57, 2017.

[52] Yanjie Wang, Zhaonan Chen, Guofen Ma, Lizhao Wang, Yanmei Liu, Meiling Qin, Xiang Fei, Yifan Wu, Min Xu, and Siyu Zhang. A frontal transcallosal inhibition loop mediates interhemispheric balance in visu-ospatial processing. Nature Communications, 14(1):5213, 2023.

[53] Sebastian Ocklenburg and Zengcai V Guo. Cross-hemispheric communication: Insights on lateralized brain functions. Neuron, 112(8):1222–1234, 2024.

[54] Petra Ritter, Michael Schirner, Anthony R McIntosh, and Viktor K Jirsa. The virtual brain integrates computational modeling and multimodal neu-roimaging. Brain connectivity, 3(2):121–145, 2013.

[55] Michael Breakspear. Dynamic models of large-scale brain activity. Nature neuroscience, 20(3):340–352, 2017.

[56] Viktor K Jirsa and Roxana A Stefanescu. Neural population modes capture biologically realistic large scale network dynamics. Bulletin of mathematical biology, 73:325–343, 2011.

[57] Roberto C Sotero, Nelson J Trujillo-Barreto, Yasser Iturria-Medina, Felix Carbonell, and Juan C Jimenez. Realistically coupled neural mass models can generate eeg rhythms. Neural computation, 19(2):478–512, 2007.

[58] John D Griffiths, Sorenza P Bastiaens, and Neda Kaboodvand. Whole-brain modelling: past, present, and future. In Computational Modelling of the Brain: Modelling Approaches to Cells, Circuits and Networks, pages 313–355. Springer, 2021.

[59] Davide Momi, Zheng Wang, Sara Parmigiani, Ezequiel Mikulan, Sorenza P Bastiaens, Mohammad P Oveisi, Kevin Kadak, Gianluca Gagli-oti, Allison C Waters, Sean Hill, et al. Stimulation mapping and whole-brain modeling reveal gradients of excitability and recurrence in cortical networks. Nature Communications, 16(1):3222, 2025.

[60] Pascal Belin, Monica Zilbovicius, Sophie Crozier, Lionel Thivard, Anne Fontaine, Marie-Cécile Masure, and Yves Samson. Lateralization of speech and auditory temporal processing. Journal of Cognitive Neuroscience, 10(4):536–540, 1998.

[61] Hugh R Wilson and Jack D Cowan. Excitatory and inhibitory interactions in localized populations of model neurons. Biophysical journal, 12(1):1–24, 1972.

[62] James Joseph Wright and David TJ Liley. Simulation of electrocortical waves. Biological cybernetics, 72:347–356, 1995.

[63] Ben H Jansen and Vincent G Rit. Electroencephalogram and visual evoked potential generation in a mathematical model of coupled cortical columns. Biological cybernetics, 73(4):357–366, 1995.

[64] Olivier David, Lee Harrison, and Karl J Friston. Modelling event-related responses in the brain. NeuroImage, 25(3):756–770, 2005.

[65] Paula Sanz Leon, Stuart A Knock, M Marmaduke Woodman, Lia Do-mide, Jochen Mersmann, Anthony R McIntosh, and Viktor Jirsa. The virtual brain: a simulator of primate brain network dynamics. Frontiers in neuroinformatics, 7:10, 2013.

[66] Viktor K Jirsa, Kelly J Jantzen, Armin Fuchs, and JA Scott Kelso. Spa-tiotemporal forward solution of the eeg and meg using network modeling. IEEE transactions on medical imaging, 21(5):493–504, 2002.

[67] Roberto C Sotero and Nelson J Trujillo-Barreto. Biophysical model for integrating neuronal activity, eeg, fmri and metabolism. Neuroimage, 39(1):290–309, 2008.

[68] Karl J Friston, Lee Harrison, and Will Penny. Dynamic causal modelling. Neuroimage, 19(4):1273–1302, 2003.

[69] Jayant Jha, Meysam Hashemi, Anirudh Nihalani Vattikonda, Huifang Wang, and Viktor Jirsa. Fully bayesian estimation of virtual brain parameters with self-tuning hamiltonian monte carlo. Machine Learning: Science and Technology, 3(3):035016, 2022.

[70] Davide Momi, Zheng Wang, and John D Griffiths. Tms-evoked responses are driven by recurrent large-scale network dynamics. Elife, 12, 2023.

[71] Norman Geschwind and Albert M Galaburda. Cerebral lateralization: Biological mechanisms, associations, and pathology: I. a hypothesis and a program for research. Archives of neurology, 42(5):428–459, 1985.

[72] Vivek V Sharma, Jennifer Vannest, and Darren S Kadis. Asymmetric information flow in brain networks supporting expressive language in childhood. Human Brain Mapping, 44(3):1062–1069, 2023.

[73] Mauro Ursino, Giulia Ricci, Laura Astolfi, Floriana Pichiorri, Manuela Petti, and Elisa Magosso. A novel method to assess motor cortex connectivity and event related desynchronization based on mass models. Brain Sciences, 11(11):1479, 2021.

[74] Daniel E Feldman. Inhibition and plasticity. Nature neuroscience, 3(4):303–304, 2000.

[75] Peter J Hellyer, Barbara Jachs, Claudia Clopath, and Robert Leech. Local inhibitory plasticity tunes macroscopic brain dynamics and allows the emergence of functional brain networks. NeuroImage, 124:85–95, 2016.

[76] Lotte J Herstel and Corette J Wierenga. Network control through coordinated inhibition. Current Opinion in Neurobiology, 67:34–41, 2021.

[77] Ryoma Hattori, Kishore V Kuchibhotla, Robert C Froemke, and Takaki Komiyama. Functions and dysfunctions of neocortical inhibitory neuron subtypes. Nature neuroscience, 20(9):1199–1208, 2017.

[78] Soohyun Lee, Illya Kruglikov, Z Josh Huang, Gord Fishell, and Bernardo Rudy. A disinhibitory circuit mediates motor integration in the somatosen-sory cortex. Nature neuroscience, 16(11):1662–1670, 2013.

[79] Carsten K Pfeffer, Mingshan Xue, Miao He, Z Josh Huang, and Massimo Scanziani. Inhibition of inhibition in visual cortex: the logic of connections between molecularly distinct interneurons. Nature neuroscience, 16(8):1068–1076, 2013.

[80] Hyun-Jae Pi, Balázs Hangya, Duda Kvitsiani, Joshua I Sanders, Z Josh Huang, and Adam Kepecs. Cortical interneurons that specialize in disin-hibitory control. Nature, 503(7477):521–524, 2013.

[81] Olivier David, Stefan J Kiebel, Lee M Harrison, Jérémie Mattout, James M Kilner, and Karl J Friston. Dynamic causal modeling of evoked responses in eeg and meg. NeuroImage, 30(4):1255–1272, 2006.

[82] Caroline A Lea-Carnall, Wael El-Deredy, Charlotte J Stagg, Stephen R Williams, and Nelson J Trujillo-Barreto. A mean-field model of glutamate and gaba synaptic dynamics for functional mrs. Neuroimage, 266:119813, 2023.

[83] Richard C Oldfield. The assessment and analysis of handedness: the edinburgh inventory. Neuropsychologia, 9(1):97–113, 1971.

[84] Arne Ewald, Sabrina Aristei, Guido Nolte, and Rasha Abdel Rahman. Brain oscillations and functional connectivity during overt language production. Frontiers in psychology, 3:166, 2012.

[85] Xing Tian and David Poeppel. The effect of imagination on stimulation: the functional specificity of efference copies in speech processing. Journal of cognitive neuroscience, 25(7):1020–1036, 2013.

[86] Xing Tian and David Poeppel. Mental imagery of speech and movement implicates the dynamics of internal forward models. Frontiers in psychology, 1:7029, 2010.

[87] Francesco Mantegna, Joan Orpella, and David Poeppel. Time-resolved hemispheric lateralization of audiomotor functional connectivity during covert speech production. Cell Reports, 44(1), 2025.

[88] Andrew Bowers, Tim Saltuklaroglu, David Jenson, Ashley Harkrider, and David Thornton. Power and phase coherence in sensorimotor mu and temporal lobe alpha components during covert and overt syllable production. Experimental brain research, 237(3):705–721, 2019.

[89] David Jenson, Andrew L Bowers, Ashley W Harkrider, David Thornton, Megan Cuellar, and Tim Saltuklaroglu. Temporal dynamics of senso-rimotor integration in speech perception and production: independent component analysis of eeg data. Frontiers in psychology, 5:656, 2014.

[90] Mark Jenkinson, Christian F Beckmann, Timothy EJ Behrens, Mark W Woolrich, and Stephen M Smith. Fsl. Neuroimage, 62(2):782–790, 2012.

[91] J-Donald Tournier, Robert Smith, David Raffelt, Rami Tabbara, Thijs Dhollander, Maximilian Pietsch, Daan Christiaens, Ben Jeurissen, Chun-Hung Yeh, and Alan Connelly. Mrtrix3: A fast, flexible and open software framework for medical image processing and visualisation. Neuroimage, 202:116137, 2019.

[92] Elias Kellner, Bibek Dhital, Valerij G Kiselev, and Marco Reisert. Gibbs-ringing artifact removal based on local subvoxel-shifts. Magnetic resonance in medicine, 76(5):1574–1581, 2016.

[93] Jelle Veraart, Dmitry S Novikov, Daan Christiaens, Benjamin Ades-Aron, Jan Sijbers, and Els Fieremans. Denoising of diffusion mri using random matrix theory. Neuroimage, 142:394–406, 2016.

[94] Jesper LR Andersson, Stefan Skare, and John Ashburner. How to correct susceptibility distortions in spin-echo echo-planar images: application to diffusion tensor imaging. Neuroimage, 20(2):870–888, 2003.

[95] Dominic Holland, Joshua M Kuperman, and Anders M Dale. Efficient correction of inhomogeneous static magnetic field-induced distortion in echo planar imaging. Neuroimage, 50(1):175–183, 2010.

[96] Jesper LR Andersson and Stamatios N Sotiropoulos. An integrated approach to correction for off-resonance effects and subject movement in diffusion mr imaging. Neuroimage, 125:1063–1078, 2016.

[97] Nicholas J Tustison, Brian B Avants, Philip A Cook, Yuanjie Zheng, Alexander Egan, Paul A Yushkevich, and James C Gee. N4itk: improved n3 bias correction. IEEE transactions on medical imaging, 29(6):1310– 1320, 2010.

[98] J-Donald Tournier, Chun-Hung Yeh, Fernando Calamante, Kuan-Hung Cho, Alan Connelly, and Ching-Po Lin. Resolving crossing fibres using constrained spherical deconvolution: validation using diffusion-weighted imaging phantom data. Neuroimage, 42(2):617–625, 2008.

[99] Robert E Smith, Jacques-Donald Tournier, Fernando Calamante, and Alan Connelly. Anatomically-constrained tractography: improved diffusion mri streamlines tractography through effective use of anatomical information. Neuroimage, 62(3):1924–1938, 2012.

[100] Robert E Smith, Jacques-Donald Tournier, Fernando Calamante, and Alan Connelly. Sift2: Enabling dense quantitative assessment of brain white matter connectivity using streamlines tractography. Neuroimage, 119:338–351, 2015.

[101] Xilin Shen, Fuyuze Tokoglu, Xenios Papademetris, and R Todd Constable. Groupwise whole-brain parcellation from resting-state fmri data for network node identification. Neuroimage, 82:403–415, 2013.

[102] Robert Oostenveld, Pascal Fries, Eric Maris, and Jan-Mathijs Schoffelen. Fieldtrip: open source software for advanced analysis of meg, eeg, and invasive electrophysiological data. Computational intelligence and neuro-science, 2011(1):156869, 2011.

[103] Guido Nolte. The magnetic lead field theorem in the quasi-static approximation and its use for magnetoencephalography forward calculation in realistic volume conductors. Physics in Medicine & Biology, 48(22):3637, 2003.

[104] Andreas Spiegler, Stefan J Kiebel, Fatihcan M Atay, and Thomas R Knösche. Bifurcation analysis of neural mass models: Impact of extrinsic inputs and dendritic time constants. NeuroImage, 52(3):1041–1058, 2010.

[105] Daniel J Felleman and David C Van Essen. Distributed hierarchical processing in the primate cerebral cortex. Cerebral cortex (New York, NY: 1991), 1(1):1–47, 1991.

[106] Diederik P Kingma. Adam: A method for stochastic optimization. arXiv preprint arXiv:1412.6980, 2014.

[107] Jack L Lancaster, Marty G Woldorff, Lawrence M Parsons, Mario Li-otti, Catarina S Freitas, Lacy Rainey, Peter V Kochunov, Dan Nickerson, Shawn A Mikiten, and Peter T Fox. Automated talairach atlas labels for functional brain mapping. Human brain mapping, 10(3):120–131, 2000.

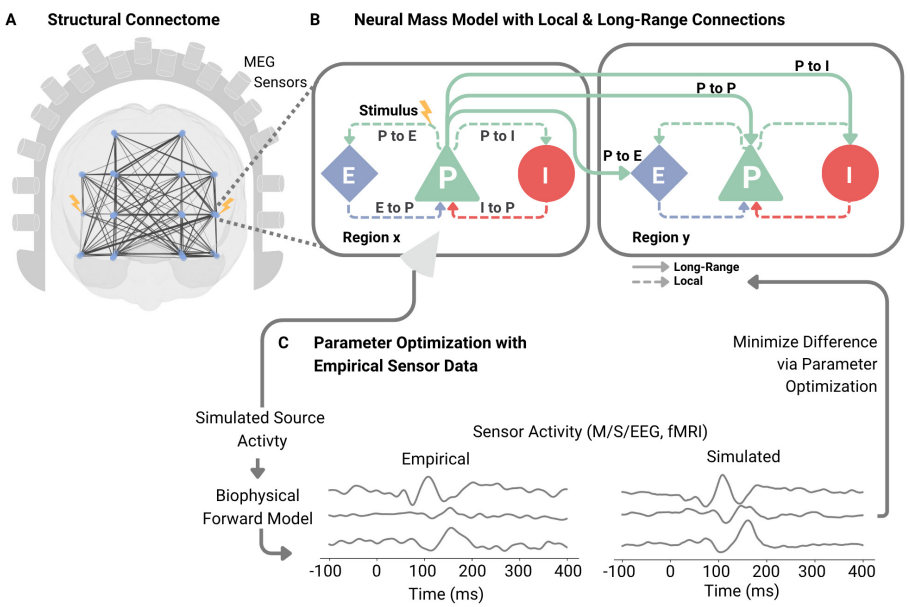


Figure 1: **Whole-brain networks of neural mass models.** (A) Structural Connectome: anatomical connectome generated from diffusion-weighted MRI tractography and T1-MRI based whole-brain atlas. Each node represents a brain region and edges represent structural connections. (B) Neural Mass Model with Local and Long-Range Connections: each region in the connectome embeds a neural mass model. Illustrated here is the Jansen-Rit model,[63, 64] comprising pyramidal (P), excitatory interneuron (E), and inhibitory interneuron (I) populations. Local (dashed lines) and long-range (solid lines) connections mediate interactions between within and between neural populations. External or sensory inputs are modeled as input injected to the pyramidal population via excitatory interneurons. (C) Parameter Optimization with Empirical Sensor Space Data: simulated membrane potentials from each region's pyramidal population are mapped to empirical data recordings (e.g., M/EEG, fMRI) using biophysical forward models. Parameters are optimized by minimizing the difference between simulated and empirical signals.

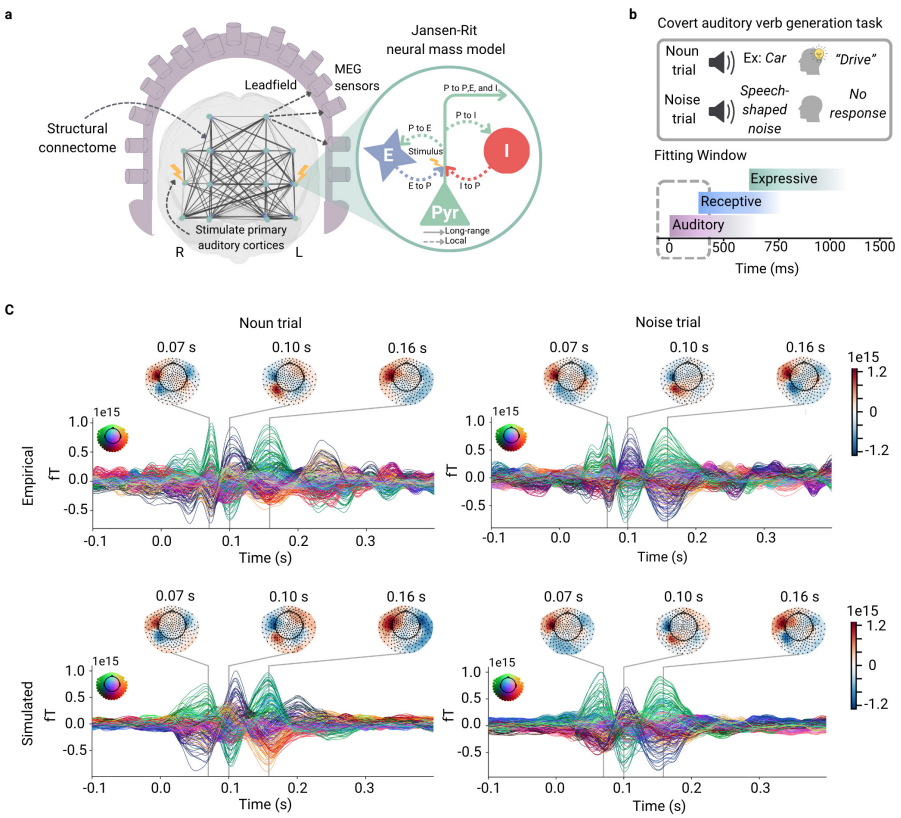


Figure 2: Individual whole-brain models simulate auditory evoked responses to linguistic and non-linguistic stimuli. (A) Schematic of the modeling framework. Subject-specific structural connectomes, derived from diffusion MRI, constrain whole-brain Jansen-Rit neural mass models. Each model simulates source-level activity projected to MEG sensors via a subject-specific leadfield. A uditory s timuli a re m odeled a s e xcitatory i nput t o p yramidal cells in bilateral primary auditory cortices. (B) Trial design for the covert auditory verb generation task, with noun (linguistic) and noise (non-linguistic) conditions. Models were fitted to early evoked responses (0–400 ms), corresponding to auditory perception prior to language production. (C) Empirical and simulated MEG responses from an exemplar subject during noun (left) and noise (right) trials. Simulations reproduce key features of early auditory evoked activity, including latency peaks (70, 100, 160 ms) and spatial distribution across sensors. Icons were created by ©Icons8, ©sparklestroke, ©pixabay, and ©Canva Creative Studio via Canva.com

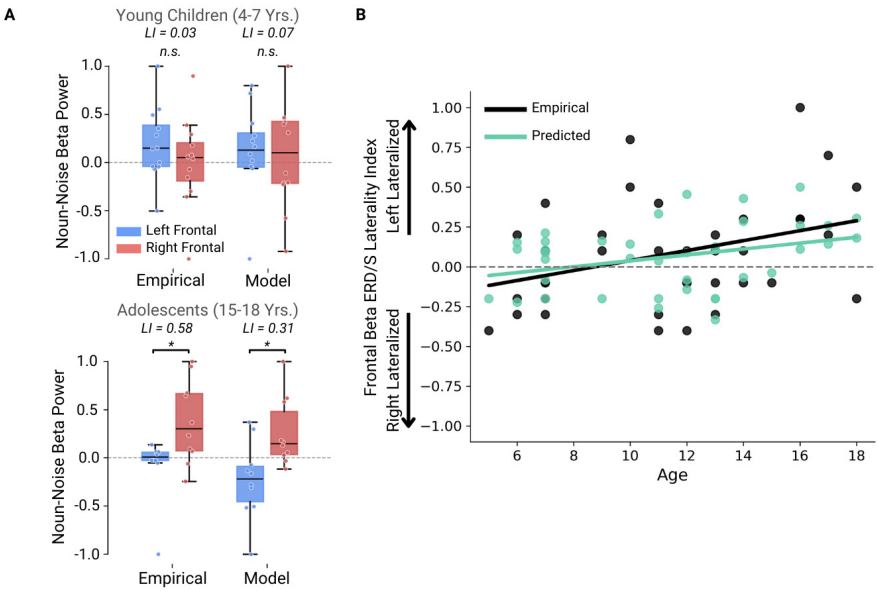


Figure 3: **Models of early auditory responses predict later lateralization of language beta ERD/S across childhood.** (A) Empirical and model-predicted frontal beta power differences (noun m inus n oise) f or young children (ages 5–7; n = 12) and adolescents (ages 15–18; n = 10). Box plots display the median (centre line), 25th and 75th percentiles (box limits), and whiskers extending to the most extreme values within 1.5×IQR. Points represent individual participants. In young children, empirical and model-predicted beta event-related desynchrony/synchrony (ERD/S) patterns were bilateral (empirical LI_{hybrid} = 0.03; predicted LI_{hybrid} = 0.07) with no significant left-right asymmetry (empirical: t(11) = 1.41, p = 0.19, two-sided paired t-test, Hedge's $g = 0.43$, 95% CI [−0.11, 0.49]; predicted: t(11) = 0.10, p = 0.92, two-sided paired t-test, Hedge's $g = 0.03$, 95% CI [−0.33, 0.36]). In adolescents, both empirical and model-predicted beta power differences s howed left-lateralization (empirical mean LI_{hybrid} = 0.59; predicted mean LI_{hybrid} = 0.31) with significant l eft–right d ifferences in th e no un–noise be ta power (empirical: t(9) = -2.36, p = 0.04, two-sided paired t-test, Hedge's $g = -1.14$, 95% CI [−0.88, −0.02] ; predicted: t(9) = -3.74, p = 0.005, two-sided paired t-test, Hedge's $g = -1.25$, 95% CI [−0.79, −0.19]). (B) Developmental trajectory of frontal beta ERD/ERS LI_{hybrid} (n = 38). Model predicted LIs correlated with age (Pearson's two-sided correlation: $r(36) = 0.33$, p = 0.043, 95% CI [0.01, 0.59]), closely replicating the empirically observed developmental trend (Pearson's two-sided correlation: $r(36) = 0.35$, p = 0.030, 95% CI [0.04, 0.60]).

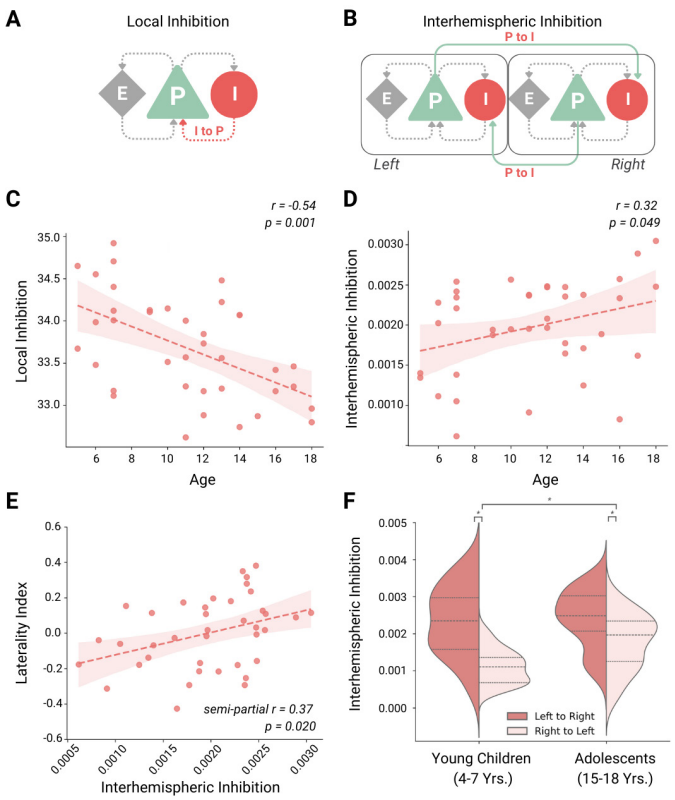


Figure 4: **Local and interhemispheric inhibitory connections during noun trials relate differently to age and language lateralization.** (A) Schematic of local inhibition quantified as the strength of the connections between inhibitory interneurons and pyramidal populations within brain regions. (B) Schematic of interhemispheric inhibition quantified as the strength of cross-hemispheric pyramidal projections to inhibitory interneurons. (C) Local inhibition significantly decreased with age (n = 38) during noun trials (Pearson's two-sided correlation: r(36) = −0.53, p < 0.001, uncorrected, 95% CI [−0.72, −0.25]). (D) Interhemispheric inhibition significantly increased with age (n = 39; Pearson's two-sided correlation: r(37) = 0.32, p = 0.0486, uncorrected, 95% CI [0.003, 0.58]). (E) Interhemispheric inhibition was significantly correlated with LI_{hybrid}, even after controlling for age (n = 39; Semi-partial two-sided correlation: r(37) = 0.37, p = 0.020, uncorrected, 95% CI [0.063, 0.62]). Shaded areas represent 95% confidence intervals. (F) Comparison of left-to-right (L2R) and right-to-left (R2L) interhemispheric inhibition between young children (n = 12) and adolescents (n = 10). Violin plots depict the kernel density distribution; dashed horizontal lines represent the 25th percentile, median, and 75th percentile. L2R inhibition was stronger than R2L inhibition in both groups (Young children: two-sided paired t-test, $t(11) = 5.81$, $p < 0.001$, 95% CI [0.0008, 0.002], Hedge's $g = 1.69$; Adolescents: two-sided paired t-test, $t(9) = 4.89$, $p < 0.001$, Hedge's $g = 0.80$, 95% CI [0.0003, 0.0009]. R2L inhibition was stronger in adolescents than in young children (Welch's two-sided independent t-test, $t(14.1) = -2.40$, $p = 0.031$, Hedge's $g = -1.03$), while L2R inhibition did not differ significantly between groups (Welch's two-sided independent t-test, $t(20.0) = -0.20$, $p = 0.844$, Hedge's $g = -0.08$). * indicates two-sided $p < 0.05$.

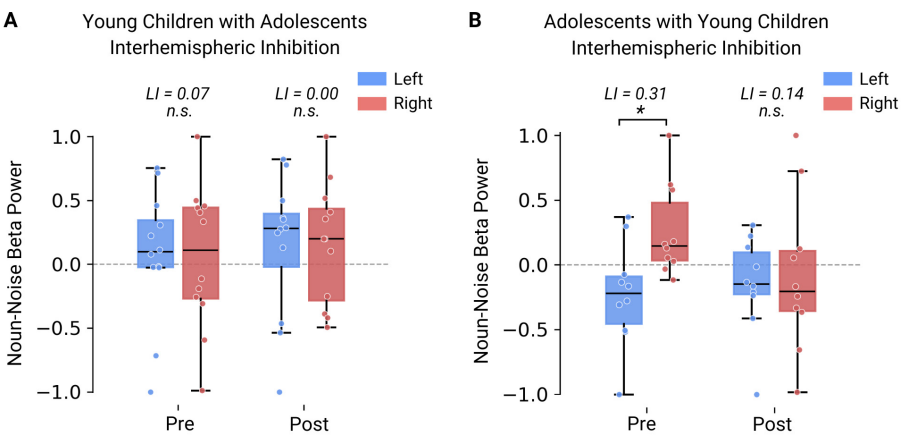


Figure 5: Virtual interhemispheric inhibitory transplants alter lateralization in adolescents, but not in young children. (A) Frontal noun-noise beta power in young children (n = 12) before and after a virtual transplant of mean frontal interhemispheric inhibitory connection strengths from adolescents. Beta patterns in young children remained bilateral, with no significant differences between the left and right frontal lobes (t(11) = -0.07, p = 0.95, two-sided paired t-test, Hedge's g = 0.03, 95% CI [-0.45, 0.42]), and the mean LI_{hybrid} remained unchanged (Pre LI_{hybrid} = 0.07; Post LI_{hybrid} = 0.0). Box plots display the median (centre line), 25th and 75th percentiles (box limits), and whiskers extending to the most extreme values within 1.5×IQR. Points represent individual participants. (B) Frontal beta power differences i n adolescents (n = 10) before and after a virtual transplant of mean frontal interhemispheric inhibitory connection strengths from young children. Post-transplant, beta patterns in adolescents became bilateral, with no significant d ifferences between the left and right frontal lobes (t(9) = -0.34, p = 0.74, two-sided paired t-test, Hedge's g = -0.13, 95% CI [-0.50, 0.37]), and the mean LI_{hybrid} decreased from 0.31 to 0.14. Reported LI_{hybrid} values reflect g roup-averaged n oun-noise beta power.

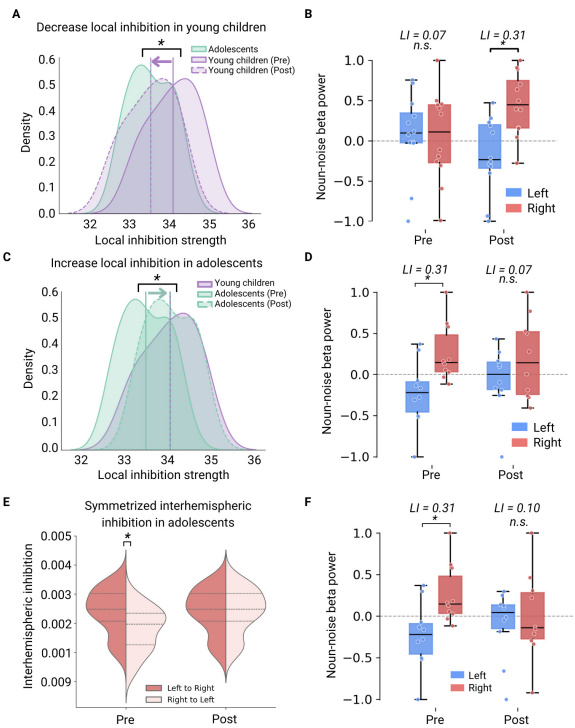


Figure 6: **Local and interhemispheric inhibition interact to drive lateralization in silico.** (A) Decreasing local inhibition in young children (n = 12) shifted their coupling strength distribution to match that of adolescents (Pre: Welch's t(19.17) = -2.73, p = 0.013, Hedge's g = -0.980, 95% CI [-0.98, -0.13]; Post: Welch's t(19.7) = 0.0, p = 1.0, Hedge's g = 0.0, 95% CI [-0.43, 0.43]). (B) Noun-noise beta power differences in young children (n = 12) before and after decrease in local inhibition. Beta patterns in young children became lateral-ized, with significant differences in noun-noise beta power between the left and right frontal lobes (t(11) = -4.18, p = 0.0015, two-sided paired t-test, Hedge's $g = -1.44$, 95% CI $[-0.97, -0.30]$), and mean LI_{hybrid} increased (Pre LI_{hybrid} = 0.07; Post LI_{hybrid} = 0.31). (C) Increasing local inhibition in adolescents (n = 10) shifted their coupling strength distribution to match that of young children (Pre: Welch's t(19.17) = -2.73, p = 0.013, Hedge's g = -0.980, 95% CI [-0.98, -0.13]; Post: Welch's t(19.7) = 0.0, p = 1.0, Hedge's g = 0.0, 95% CI [-0.43, 0.43]). * indicates two-sided p < 0.05. (D) Noun-noise beta power in adolescents (n = 10) before and after increase in local inhibition. Beta patterns in adolescents became bilateral, with no significant differences between the left and right frontal lobes (t(9) = -1.47, p = 0.18 , two-sided paired t-test, Hedge's $g = -0.56$, 95% CI $[-0.65, 0.14]$), and mean LI_{hybrid} decreased (Pre LI_{hybrid} = 0.31; Post LI_{hybrid}= 0.07). Box plots display the median (centre line), 25th and 75th percentiles (box limits), and whiskers extending to the most extreme values within 1.5×IQR. Points represent individual participants. (E) Interhemi-spheric inhibition in adolescents (n = 10) pre-and post-symmetrization, where left-to-right P-I Coupling strength is mirrored in the right-to-left connections, * indicates two-sided p < 0.05. Violin plots depict the kernel density distribution; dashed horizontal lines represent the 25th percentile, median, and 75th percentile. (F) Noun-noise beta power in adolescents (n =10) before and after symmetrized interhemispheric inhibition. Beta patterns in adolescents became bilateral (Pre LI_{hybrid}= 0.31; Post LI_{hybrid} = 0.10), with no significant differences between the left and right frontal lobes ($t(9) = -0.84$, $p = 0.42$, two-sided paired t-test, Hedge's $g = -0.19$, 95% CI $[-0.3464, 0.1584]$).